Available online at www.sciencedirect.com

ScienceDirect

Procedia Engineering 103 (2015) 577 – 584

Procedia Engineering

www.elsevier.com/locate/procedia

The 13th Hypervelocity Impact Symposium

Modeling Momentum Transfer from Kinetic Impacts: Implications for Redirecting Asteroids

A.M. Stickle*[,a], J.A. Atchison[a], O.S. Barnouin[a], A.F. Cheng[a], D.A. Crawford[b], C.M. Ernst[a], Z. Fletcher[a], and A.S. Rivkin[a]

[a]*Johns Hopkins University Applied Physics Laboratory, Laurel, MD 20723, USA*
[b]*Sandia National Laboratories, Albuquerque, NM 87185, USA*

Abstract

Kinetic impactors are one way to deflect a potentially hazardous object headed for Earth. The Asteroid Impact and Deflection Assessment (AIDA) mission is designed to test the effectiveness of this approach and is a joint effort between NASA and ESA. The NASA-led portion is the Double Asteroid Redirect Test (DART) and is composed of a ~300-kg spacecraft designed to impact the moon of the binary system 65803 Didymos. The deflection of the moon will be measured by the ESA-led Asteroid Impact Mission (AIM) (which will characterize the moon) and from ground-based observations. Because the material properties and internal structure of the target are poorly constrained, however, analytical models and numerical simulations must be used to understand the range of potential outcomes. Here, we describe a modeling effort combining analytical models and CTH simulations to determine possible outcomes of the DART impact. We examine a wide parameter space and provide predictions for crater size, ejecta mass, and momentum transfer following the impact into the moon of the Didymos system. For impacts into "realistic" asteroid types, these models produce craters with diameters on the order of 10 m, an imparted Δv of 0.5–2 mm/s and a momentum enhancement of 1.07 to 5 for a highly porous aggregate to a fully dense rock.

Peer-review under responsibility of the Curators of the University of Missouri On behalf of the Missouri University of Science and Technology

Keywords: Kinetic Impactors; CTH models; Didymos; AIDA mission concept

1. Introduction

There are roughly 1000 near-Earth objects with sizes > 1 km, any of which would have civilization-wide consequences if they were to impact the Earth. Even smaller objects, such as that responsible for the 1908 Tunguska fireball, can devastate entire regions. Given sufficient notice, however, there are several notional mechanisms for deflecting these objects: "gravity tractors", exploitation of Yarkovsky effects, and more active techniques such as nuclear weapons and kinetic impactors. The Asteroid Impact and Deflection Assessment (AIDA) mission is a joint concept between NASA and ESA designed to test the effectiveness of a kinetic impactor. The mission is composed of two independent, but mutually supportive, components: the NASA-led Double Asteroid Redirect Test (DART), and the ESA-led Asteroid Impact Mission (AIM). The spacecraft will be sent to the near-Earth binary asteroid 65803 Didymos, which makes close approaches to Earth in 2022 and 2024. These close approaches make it an ideal target for a kinetic impactor asteroid deflection demonstration as it will be easily observable from Earth. The kinetic impactor (the 2-m x 2-m x 2-m, 300 kg DART spacecraft) will impact the small moon (~150 m in diameter, here called "Didymoon") of the binary system at 6.25 km/s. The deflection of the moon will be measured by the AIM spacecraft and from ground-based observations by measuring the

* Angela Stickle. Tel.: +1-240-228-3822; fax: +1-240-228-8939.
E-mail address: angela.stickle@jhuapl.edu.

Peer-review under responsibility of the Curators of the University of Missouri On behalf of the Missouri University of Science and Technology
doi:10.1016/j.proeng.2015.04.075

change in the moon's orbital period. The intent is to hit the moon in the equatorial plane near the COF to transfer momentum into a change in the orbital period rather than inclination or rotation. Here we describe preliminary studies of expected outcomes of the DART impact experiment.

1.1. The DART Spacecraft and Trajectory

The DART spacecraft must impact the target asteroid in a direction that maximizes the imparted orbital period change. This drives the arrival relative velocity into Didymoon's orbit plane relative to Didymos. In addition, the lighting must be favorable for approach optical navigation to ensure that the target can be identified and differentiated from the primary asteroid. In the 2019 to 2022 timeframe, four launch periods offer direct chemical trajectories that meet these requirements, each leading to impact on 01 October 2022. The transfer trajectories depart with high declination of launch asymptotes, which provide the required change in inclination between Earth and Didymos. The trajectories impact the asteroid near its close approach with Earth, below the ecliptic plane. This orientation requires relatively low launch energy and enables low cost launch vehicle options. A sample trajectory launching in December 2021 is illustrated in Figure 1. The only required maneuvers are associated with launch correction and statistical targeting updates.

The asteroid will be targeted using a combination of ground-controlled optical navigation and on-board autonomous navigation. The primary asteroid will be visible for months prior to arrival, enabling corrective maneuvers to ensure that the spacecraft will arrive at the system. On arrival, the spacecraft will transition to autonomous image processing and targeting algorithms. This is primarily because the two asteroids can't be reliably differentiated until ~2–4 hours prior to impact, when the dim secondary asteroid is separated from the primary asteroid by at least 2 pixels (roughly the width of the simulated point-spread function).

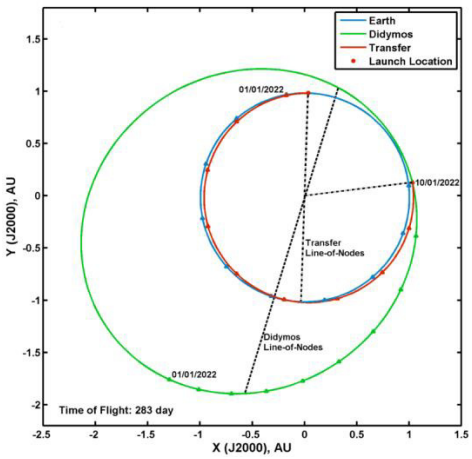

Fig. 1. Sample DART trajectory to impact Didymoon on 01 October 2022.

2. Methods

2.1. Analytical Models and Scaling Predictions

The analytical calculations of momentum transfer and crater size are based on well-known scaling relationships developed from studying laboratory impact craters (e.g., [4]) that give reasonable estimates for cratering efficiency and size. We computed the crater size, estimated the amount of ejecta, momentum transfer and change in velocity (Δv) for various target types, including a strong rock, a weakly cemented rock, a highly porous weak rock, and a cohesionless sand-like surface, following the approach outlined in [5–8] to account for ejecta retained by the target body. Results of these calculations for the different target types are shown in Tables 1 and 2 in section 3. These calculations assume the impactor is an aluminum sphere of equivalent mass to the DART spacecraft impacting at a 90-degree angle to the surface at 6.25 km/s.

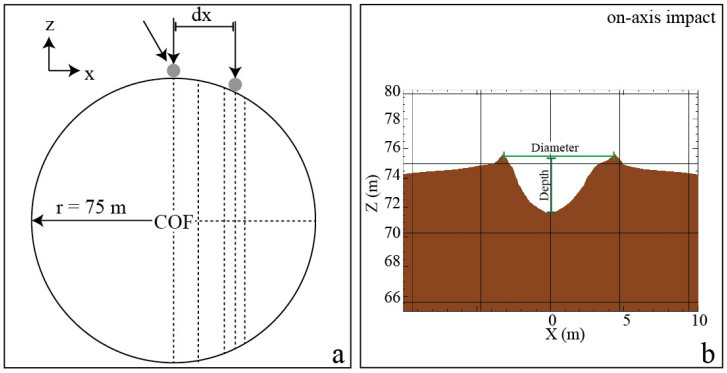

Fig. 2. a) Schematic of CTH model setup and location of Lagrangian tracers. The z direction is the assumed orbit trajectory of Didymoon. b) Diagram of depth and diameter measurements from final craters.

2.2. CTH Model Description

To better understand the large parameter space and possible outcomes of the DART impact, simulations of the event were also performed using the CTH hydrocode from Sandia National Laboratories [1]. Because the physical properties of the Didymos system are not well constrained, we examined a variety of target properties and impact scenarios to explore the expected results of the DART impact (Tables 1–3). Mission design constraints define an impact velocity and a likely impact location with respect to the center of figure (COF) of Didymoon. However, impact angle (whether due to an inclined trajectory or to local surface topography) is not well constrained. To better inform mission design, we examined the effects of material properties, impact location (e.g., where DART impacts with respect to the COF), and impact angle on momentum transfer.

Simulations were performed in a 2-D or 3-D rectangular coordinate system. Two-dimensional models were used for vertical (normal with respect to the surface) impacts through the COF of Didymoon, while 3D models allowed for oblique impacts or impacts offset from the COF. Adaptive Mesh Refinement [2] was used to obtain high-resolution coverage of important areas while lessening computer resource usage. These simulations have a maximum resolution of ~3 cm, with nominal resolution of ~15 cm. To further optimize computing resources, the DART spacecraft was modeled as a solid aluminum cylinder (2D) or sphere (3D) with a radius of 32.5 cm. Impacting at 6.25 km/s, this simplification provided the correct impact energy for the ~300-kg DART spacecraft. The spacecraft is modeled using an ANEOS equation of state for aluminum 2024 and a Johnson-Cook plasticity model. Because the shape of Didymoon is unknown, here the moon was modeled as a spherical, 150-m-diameter rocky body, using a SESAME equation of state for a basalt-like material (ρ=2.82 g/cm^3 for a fully competent, strong material). In some cases, the p-α model for porosity was included to simulate initial porosity to match the measured density of the Didymos system (ρ=1.7 g/cm^3) with crush-curve parameters for pumice from [3]. A pressure-dependent yield surface was used to model the deformation behavior of Didymoon, and the strength parameters were chosen to represent the range of possible material properties (similar to those used in the analytical models, section 2.2). The models described below have a yield strength of either 2 or 200 MPa. The simulations were run to a stop time of 0.4–0.5 seconds, a time by which the crater stopped forming and reverberations in the body from the shock wave had nearly stopped. The long run time minimized the noise in the velocity measured by tracer particles.

The momentum transferred to the asteroid by the spacecraft is parameterized by β, the momentum enhancement of the moon, by adding the initial spacecraft momentum to the momentum of the ejecta excavated during crater formation. In each CTH simulation, the moon was seeded with nearly 1000 Lagrangian tracer particles (selected tracers shown in Figure 2a) that tracked the velocity and state of the material (e.g., pressure, temperature, density) through time following impact. Because the moon was initially at rest, the velocity of the tracers following impact was tracked and used to calculate Didymoon's momentum after impact. The resultant momentum transfer, β, to the moon was then calculated by:

$$\beta = 1 + \frac{p_{moon}}{p_{spacecraft}} \tag{1}$$

where p_{moon} is the momentum of the moon following impact ($v_z^{avg} * m_{moon}$), and $p_{spacecraft}$ is the initial momentum of the

spacecraft.

The depth and diameter of the craters were also measured from the CTH models for different impact scenarios. The calculation was run until the crater geometry had stopped evolving. The diameter was measured as the rim-to-rim distance from a 2-D slice through the center plane of the 3-D models, here always measured in the *XZ* plane. The depth was measured from the center of the crater at the height of the rim to the floor of the crater (Figure 2b).

3. Analytical Models

Table 1. Parameter space calculations. Values of μ, K_1, and $\overline{Y}$ for strengthless sand, dry and wet soil, and soft and hard rock are taken from [4]. The box indicates the most likely range of scenarios when the asteroid is considered to possess low to moderate porosity of 30–40% similar to sand.

Strength Properties	μ	K_1	Y (MPa)	Final Crater Diameter (m)	Mass escaping moon (kg)	% of equivalent crater 'mass'	Mass escaping system (kg)	% of equivalent crater 'mass'
sand	0.41	0.24	0	114	1.10E+07	6.45%	1.55E+06	0.91%
sand	0.41	0.24	4.0E-6	98	6.69E+06	6.25%	9.78E+05	0.91%
sand	0.41	0.24	1.0E-5	86	7.37E+06	10.32%	1.13E+06	1.59%
sand	0.41	0.24	9.0E-5	56	5.02E+06	24.72%	1.21E+06	5.95%
sand	0.41	0.24	1.0E-4	55	4.83E+06	25.33%	1.20E+06	6.29%
sand	0.41	0.24	1.0E-3	34	1.50E+06	32.32%	9.05E+05	19.45%
sand	0.41	0.24	0.010	21	3.76E+06	33.24%	3.47E+05	30.75%
sand	0.41	0.24	0.100	13	9.14E+04	33.35%	9.09E+04	33.14%
sand	0.41	0.24	1.000	8	2.22E+04	33.3%	2.22E+04	33.35%
dry soil	0.41	0.24	0.180	12	6.38E+04	33.39%	6.34E+04	33.18%
wet soil	0.55	0.2	1.140	17	1.71E+05	33.41%	1.71E+05	33.41%
soft rock	0.55	0.2	7.600	10	4.51E+04	44.21%	4.51E+04	44.21%
hard rock	0.55	0.2	18.000	8	1.76E+04	33.43%	1.76E+04	33.43%

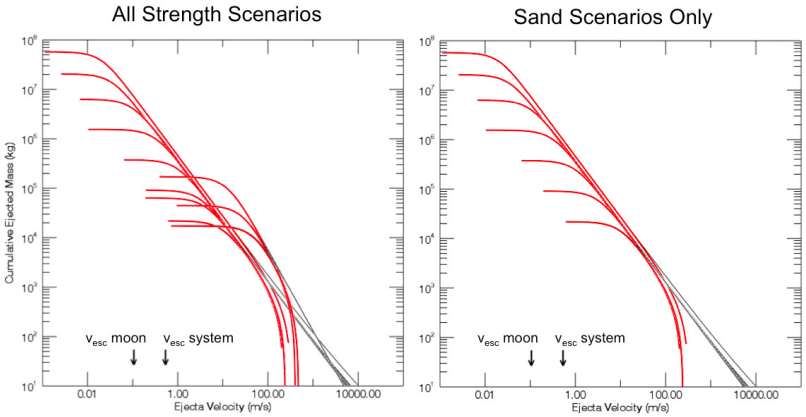

Fig. 3. Cumulative ejected mass versus ejecta velocity for a range of DART impact scenarios.

We use crater scaling rules [5–8] to calculate the amount of ejecta expected to escape the moon and the asteroid system and to predict the size of the final crater. Because the physical properties of the target are not well constrained, we explore the possible outcomes of the impact event for a range of material properties. The transition between strength- and gravity-dominated cratering events can be estimated by equating non-dimensionalized crater scaling terms π_2 and π_3:

$$\pi_2 = \left(\frac{g a_i}{v_i^2}\right) \quad and \quad \pi_3 = \left(\frac{\bar{Y}}{\rho_t v_i^2}\right) \tag{2}$$

In order for the cratering process to be gravity dominated, the effective strength of the moon would have to be ~4 Pa. Therefore, the DART impact into the moon of Didymos will be a strength-dominated event. We consider a range of possible material strength values for the moon, which are listed in Table 1. Gravity-dominated crater scaling rules provide upper-limits for the calculations. In these models, we do not consider porosity.

Following the work of [5–8], the size of the crater is calculated using the cratering efficiency term, π_v, to calculate the excavated crater volume, which is then used to determine a transient crater radius:

$$\pi_v = K_1 \left(\pi_2 \pi_4^{-1/3} + \pi_3^{\frac{2+\mu}{2}} \right)^{-3\mu/(2+\mu)} \tag{3}$$

where μ is an empirically determined variable between 1/3 and 2/3 and π_4 is the ratio of the target and impactor densities. We can equate two equations to determine crater volume:

$$V = \pi_v \left(\frac{m_i}{\rho_t}\right) = c_1 \pi R^3 \quad and \quad R = \left(\frac{V}{c_1 \pi}\right)^{1/3} \tag{4}$$

where where c_1 ~0.25 to 0.33 and R is the transient crater radius. We multiply R by 1.25 to convert from transient to rim-to-rim radius.

Again, following the work of [5–8], we investigate the amount of ejecta that will be produced by the event. We first calculate the ejecta velocity as a function of emergence position. Because the cratering activity needs to be "shut off" when the power-law scaling no longer works, we calculate an effective velocity (v_{ef}) at a given distance from the impact point (x) after losses due to gravity and strength:

$$v_{ef}(x) = \left[v_{ej}^2 - C_{vpg}^2 g x - C_{vps}^2 \frac{\bar{Y}}{\rho_t} \right]^{\frac{1}{2}} \tag{5}$$

where C_{vps} and C_{vpg} are constants related to μ and the shape of the transient crater. To calculate the mass of excavated material in a given shell of the transient crater located between x_{n+1} and x_n from the crater center, we use the equation:

$$m_{ri} = \frac{1}{9} \pi \rho_t \left(x_{n+1}^3 - x_n^3 \right) \tag{6}$$

where it is assumed that the excavation depth of the transient crater is approximately equal to 1/9 of the transient crater diameter. Figure 3 illustrates the relationship between the calculated v_{ef} and the cumulative mass of material ejected at or below a given v_{ef}. The results of the calculations for all scenarios are listed in Table 1. The most likely range of scenarios is outlined by the box and result in a final crater size between 8 and 17 m and a cumulative mass of escaping ejecta between ~10^4 and 10^5 kg.

Using the scaling relationships above and a correction for ejecta retained by the target asteroid [5], we also computed the momentum transfer and change in velocity (Δv) for four target types: a strong rock, a weakly cemented rock, a highly porous weak rock, and a cohesionless sand-like surface. This method expands on results above by including the effects of porous material with μ=0.4. The most likely scenario for Didymoon's material properties is that of highly porous rock that possesses some strength. This is because the moon of a binary asteroid is likely the result of re-accreting regolith that was shed by the parent binary to produce a loosely bound, highly porosity moon [e.g., 9]. Results of these calculations for the different target types are shown in Table 2.

Table 2. Analytical predictions of momentum transfer and Δv imparted to an asteroid after the DART impact, including the effects of porosity

Material	Asteroid density (kg/m^3)	Effective strength (kPa)	β	Δv (mm/s)
Competent rock	3000	300	5.00	1.76
Weakly cemented rock	2600	200	1.31	0.53
Highly porous,weak	1000	2	1.49	3.16
Cohesionless sand	1700	0	2.05	4.26

4. CTH models

4.1. Crater Geometry

Initially, 2-D models were used to simulate vertical impacts through the COF of Didymoon for both fully dense and porous targets. The final crater formed following the impact of a solid aluminum sphere representing the DART spacecraft into a fully porous body has a depth and diameter of 2.5 m and 14.5 m, respectively. The crater floor is uplifted, and the final structure is shallow and wide compared to impacts into more dense targets (Fig. 4) for this impact scenario.

Figure 4 shows the final crater geometry from four different 3-D models, including impacts through the COF and various distances away. Each scenario results in a slightly different crater shape and size (Table 3). The three fully dense models all have similar-sized final craters, but the model with an initial density of 1.7 g/cm^3 (i.e., higher porosity) forms a much smaller crater with steeper walls. As the impact gets farther from the COF of Didymoon, the effective impact angle becomes more oblique, resulting in an asymmetric crater. This will have important implications for the ejecta trajectories, and thus the momentum transfer to Didymoon. For increasingly oblique impacts, ejecta are concentrated downrange [e.g., 9] (here, the x direction), which lessens the thrust from the ejecta in the orbit direction.

For "realistic" material properties (sand-weak/soft rock), the analytical models predicted crater diameters between 8 and 17 m. Specifically, the models of weak rock, with yield strength of 7.6 MPa, predict crater diameters of 12 m, while "sand" with yield strength of 1 MPa predict a crater diameter of 8 m. For equivalent impacts (90°, through the COF), the range predicted by these CTH simulations is 6–15 km, a difference of 12–25% from the analytical predictions.

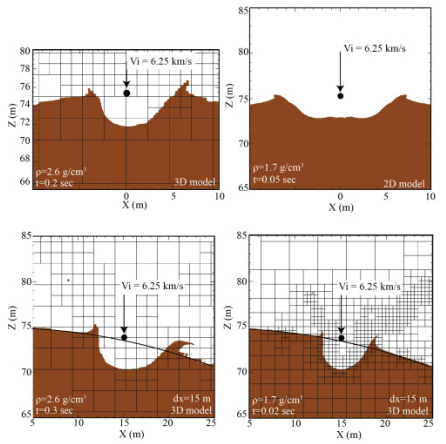

Fig. 4. Final crater sizes for differing initial impact scenarios. All models were run in a 3-D rectangular coordinate system. Craters finish forming more quickly in models including porosity (bottom right), and they are smaller than in the fully dense case. The grid lines show the effect of AMR on the resolution, with higher resolution around the ejecta. The initial impact location, projectile size and velocity are shown for reference. The black circle represents the original surface of the moon.

Table 3. Crater depth and diameter measured from CTH models for various impact scenarios

Projectile	Model Geometry	Impact location	Porosity?	Crater Depth [m]	Crater Diameter [m]
Sphere	2D	COF	Yes	2.5	14.5
Cylinder	2D	COF	No	2.1-3.1	6-9
Sphere	3D	COF	No	3.15	7.75
Sphere	3D	COF	Yes	3.8	6.4
Sphere	3D	dx=15 m	No	4.1	9
Sphere	3D	dx=15 m	Yes	3.4	5.3

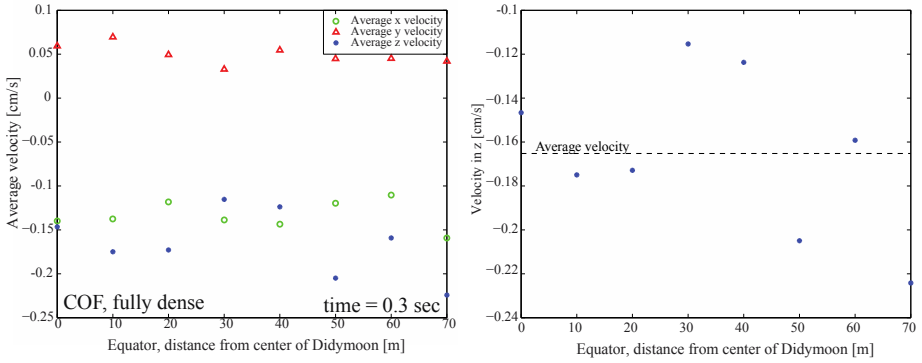

Fig. 5. (left) Velocity components along the equator of Didymoon, calculated from Lagrangian tracers at the end of one calculation. The COF is at a distance of 0 m along the equator; (right) Symbols show velocity in the direction of Didymoon's orbital motion of specific tracers along the equator of Didymoon at the end of the calculation, while the dashed line gives the average v_z of the equator.

4.2. Velocity Change and Momentum Enhancement

Table 4. CTH results for the change in velocity and momentum transfer to the moon following the DART impact

Parameter	Vz COF [cm/s]	β from COF vel (VzCOF*m)	β from equator vel (Vzeq*m)
COF	-0.147	3.8	4.2
dx=15 m	-0.224	5.4	4.8
dx=30 m	-0.229	5.5	5.7
COF porous	-0.007	1.08	1.15
dx=15m porous	-0.006	1	1.07

Preliminary results of momentum transfer from the 3-D CTH models for a fully competent, strong (yield strength of 200 MPa) moon generally agree with predictions from analytical studies. For fully dense, competent, strong rocks, we calculate values for β between approximately 3.8 and 5.5, with an imparted Δv of 1.47–2.29 mm/s to the moon for impacts at various distances (*dx*) from the COF (*dx*=0–30 m) (Table 4). These β values compare favorably with the analytical solutions shown in Table 2 for the competent rock, indicating that the impact location with respect to the COF will affect the momentum transfer in the direction of interest (in the ecliptic plane, along the direction of motion, here assumed to be the z-direction). When porosity is added to the numerical models, the calculated β values drops below those estimated for the porous analytical case, and can be as small as β ~1.

Table 4 shows a summary of imparted Δv_z and the calculated β for five impact scenarios; v_z was calculated by averaging the velocity over select tracers embedded within the moon at the end of the calculation. Two separate velocities were chosen for comparison: the velocity at the COF of the moon, as well as the average velocity along the equator of the moon (Figure 5). These velocities were then multiplied by the mass of Didymoon to calculate the momentum. All five scenarios assumed a vertical impact into Didymoon (e.g., Figure 4), though offset impacts are oblique to the surface. This will affect the momentum transferred along the preferred axis of the moon because the ejecta distribution and the resulting momentum enhancement from ejecta motion will not be symmetrical. Further, any impact offset from the COF of the body will likely impart some rotation to the body, lessening the linear momentum transferred by the impact.

4.3. Complications and Future Studies

These first order CTH models are generally consistent with the analytical predictions. However, these models are necessarily simplified from the actual likely impact scenario, and the additional complexities in the actual impact (e.g., spacecraft shape and structure, oblateness of the moon, unknown interior structure of the moon, obliquity of the impact) may affect the outcomes of the impact. Similarly, the simulations described here only cover a small percentage of the available parameter space, and future studies will explore the effects of differing amounts of porosity and different material strengths. Simulations of the expected impact with different projectile geometries are likely to yield different results; preliminary simulations of a hollow cubic spacecraft (beam structures with aluminum face sheets) result in final craters with very different shapes and much higher ejecta ejection angles. Further studies will focus on these effects in more detail, as the actual spacecraft impact will likely be nearer to this scenario.

5. Conclusions

The AIDA mission represents a unique opportunity to study a binary system in depth and to perform the first kinetic impactor experiment. Analytical models coupled with CTH simulations of the DART impact provide important insights into the expected crater size, ejecta mass, and momentum transfer from the impact. Because the target parameters are not well constrained, a large parameter space is being examined and a portion of those results are shown here. CTH simulations and analytical models provide similar predictions for crater size and momentum transfer following impact. The models are necessarily oversimplified, however they provide a first order understanding of what we may expect. For impacts into "realistic" asteroid types, the DART impact will likely generate an approximately 10-m-diameter crater and impart a velocity change of 1–2 mm/s to the moon of Didymos. This results in a momentum enhancement, β, of 3–5 for fully dense materials, and closer to 1 for highly porous material.

Acknowledgements

This work was funded under a grant from NASA in support of the NASA-ESA AIDA mission concept study. D.A. Crawford acknowledges that Sandia is a multi-program laboratory operated by Sandia Corporation, a Lockheed Martin Company, for the United States Department of Energy under Contract DE-AC04-94AL85000.

References

[1] McGlaun, J. M., Thompson, S.L., and Elrick, M.G., 1990. CTH: A three-dimensional shock wave physics code, International Journal of Impact Engineering, 10(1-4), p. 351-360.
[2] Crawford, D.A. et al. 2006. Adaptive Mesh Refinement in the CTH Shock Physics Hydrocode, The Russian Journal of Physical Chemistry B, 25:9, p. 85-90.
[3] Jutzi, M., Benz, W., and Michel P., 2008. Numerical simulations of impacts involving porous bodies I. Implementing sub-resolution porosity in a 3D SPH hydrocode, Icarus, p. 242-255.
[4] Holsapple, K.A., 1993. The scaling of impact processes in planetary sciences, Annual Review of Earth and Planetary Science 21, p. 333–373.
[5] Holsapple, K.A., Housen, K.R., 2012. Momentum transfer in asteroid impacts. I. Theory and scaling, Icarus 221, p. 875-887.
[6] Housen, K.R., Schmidt, R.M., Holsapple, K.A., 1983. Crater ejecta scaling laws: Fundamental forms based on dimensional analysis, Journal of Geophysical Research 88, p. 2485–2499.
[7] Richardson, J. E., Melosh, H.J., Lisse, C. M., and Carcich, B., 2007, A ballistics analysis of the Deep Impact ejecta plume: Determining Comet Tempel 1's gravity, mass, and density, Icarus, 190(2), 357–390, doi:10.1016/j.icarus.2007.08.001.
[8] Housen, K.R., Holsapple, K.A., 2011. Ejecta from impact craters, Icarus 211, p. 856–875.
[9] Walsh, K.J., Richardson, D.C. & Michel, P., 2008. Rotational breakup as the origin of small binary asteroids. *Nature*, 454(7), pp.188–191.
[10] Anderson, J.L.B, Schultz, P.H, Heineck, J.T., 2003. Asymmetry of ejecta flow during oblique impacts using three-dimensional particle image velocimetry, Journal of Geophysical Research 108, E8, doi: 10.1029/2003JE002075